ACS Synthetic Biology

Research Article

pubs.acs.org/synthbio

Automated Design of Programmable Enzyme-Driven DNA Circuits

Hendrik W. H. van Roekel,[†,‡] Lenny H. H. Meijer,[†,‡] Saeed Masroor,[†,§] Zandra C. Félix Garza,[‡] André Estévez-Torres,[⊥] Yannick Rondelez,[∥] Antonios Zagaris,[▽] Mark A. Peletier,[†,§] Peter A. J. Hilbers,[†,‡] and Tom F. A. de Greef*[,†,‡]

[†]Institute for Complex Molecular Systems, [‡]Department of Biomedical Engineering, Computational Biology Group, and [§]Department of Mathematics and Computer Science, Eindhoven University of Technology, P.O. Box 513, 5600 MB Eindhoven, The Netherlands

[⊥]Laboratoire de Photonique et de Nanostructures, CNRS, route de Nozay, 91460 Marcoussis, France

[∥]LIMMS/CNRS-IIS, Institute of Industrial Science, University of Tokyo, Komaba 4-6-1 Meguro-ku, Tokyo 153-8505, Japan

[▽]Department of Applied Mathematics, University of Twente, P.O. Box 217, 7500 AE Enschede, The Netherlands

Supporting Information

ABSTRACT: Molecular programming allows for the bottom-up engineering of biochemical reaction networks in a controlled *in vitro* setting. These engineered biochemical reaction networks yield important insight in the design principles of biological systems and can potentially enrich molecular diagnostic systems. The DNA polymerase−nickase−exonuclease (PEN) toolbox has recently been used to program oscillatory and bistable biochemical networks using a minimal number of components. Previous work has reported the automatic construction of *in silico* descriptions of biochemical networks derived from the PEN toolbox, paving the way for generating networks of arbitrary size and complexity *in vitro*. Here, we report an automated approach that further bridges the gap between an *in silico* description and *in vitro* realization. A biochemical network of arbitrary complexity can be globally screened for parameter values that display the desired function and combining this approach with robustness analysis further increases the chance of successful *in vitro* implementation. Moreover, we present an automated design procedure for generating optimal DNA sequences, exhibiting key characteristics deduced from the *in silico* analysis. Our *in silico* method has been tested on a previously reported network, the Oligator, and has also been applied to the design of a reaction network capable of displaying adaptation in one of its components. Finally, we experimentally characterize unproductive sequestration of the exonuclease to phosphorothioate protected ssDNA strands. The strong nonlinearities in the degradation of active components caused by this unintended cross-coupling are shown computationally to have a positive effect on adaptation quality.

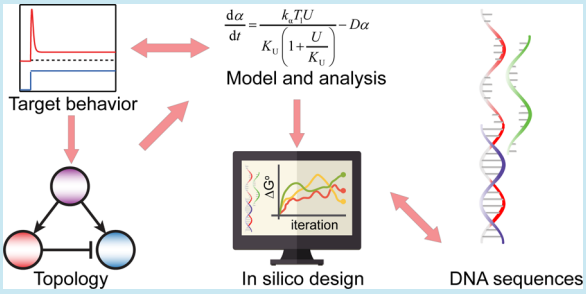

KEYWORDS: *bottom-up synthetic biology, chemical reaction networks, in vitro, in silico, DNA sequence design, cross-talk*

Biological systems are hierarchically organized networks in which each level displays internalized self-regulation while coupled to the external environment.[1] Specifically, interactions between the hierarchical layers are a key feature of the reaction networks underlying replication, protein production, energy metabolism, and organelle control.[2] Attempts to unravel the hierarchy and the exact mechanisms governing such biological processes can roughly be classified as top-down or bottom-up approaches.[3] The former tries to infer full biological networks in their natural context qualitatively at the expense of accuracy, while the latter aims at describing and understanding components of smaller size quantitatively at the expense of system complexity.[4,5] The sophisticated character of biological systems is to a great extent regulated through complex biochemical reactions networks (CRNs). The molecular components of such reaction networks interact in a dynamic manner to sense, to respond and to adapt to external signals, for example, via signaling cascades.[6] Recently, the programmability of CRNs has been demonstrated with genetic engineering of bacterial colonies.[7−9] However, engineering these CRNs in a cellular environment leads to cross-talk with the host housekeeping functions that is not always trivial to circumvent; therefore, the study of minimal biological systems in an isolated or *in vitro* fashion is an ongoing area of research.[10,11]

Employing a bottom-up approach to synthetic biology of minimal systems in an *in vitro* setting enables study of CRNs in a modular fashion. DNA-based CRNs have proven to be highly programmable and amenable for such bottom-up design strategies.[12,13] Moreover, isolation of the molecular machinery for DNA replication and transcription−translation machinery in a test tube,[14,15] followed by compartmentalization of these processes in droplets and liposomes, has opened the door toward functional artificial cells.[16] Harnessing the dissipative transcription−translation machinery in an open system

Received: August 14, 2014

dx.doi.org/10.1021/sb500300d | *ACS Synth. Biol.* XXXX, XXX, XXX−XXX

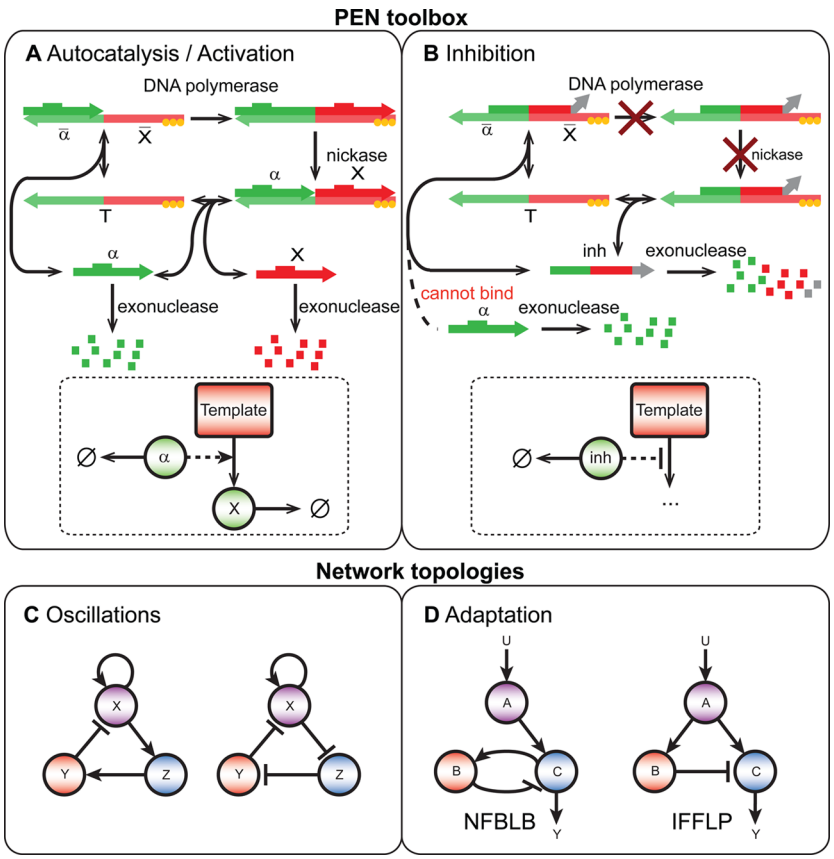

Figure 1. Bottom-up engineering of *in vitro* biochemical reaction networks using the polymerase−exonuclease−nickase (PEN) toolbox. (A) Activation of a protected template: oligomer α binds to its complementary part $\overline{\alpha}$ on template T. DNA polymerase then extends the primed template with sequence X complementary to $\overline{X}$ resulting in fully hybridized dsDNA. Oligomer α contains a nicking enzyme recognition site. Because the temperature is close to the melting temperature of the primer−template complex, nicking of the fully hybridized dsDNA results in two oligomers α and X that can readily dissociate from the template. Depending on the choice of the sequence of oligomer X, the template can function as an autocatalytic node, that is, $X = \alpha$, a delay node, that is, $X = \beta$ or an inhibitory node, that is, $X = inh$. The yellow dots on the template strands indicate a phosphorothioate modified backbone at the 5′ end, protecting the template from degradation by exonuclease. (B) Inhibition of a template: an inhibitory oligomer *inh* binds strongly to a template, rendering it inactive. Enzymes cannot act on the inactive template, as the nicking enzyme recognition site is not fully displayed, and a two base mismatch at the 3′ end prevents DNA polymerase from extending oligomer *inh*. (C) Short-range activation combined with delayed inhibition is a common design motif to construct oscillatory biochemical circuits.[17,24,30,42] (D) The negative feedback loop with a buffer node (NFBLB) and the incoherent feedforward loop with a proportioner node (IFFLP) can display adaptation.[40] The network topologies presented in C and D can be constructed using the PEN toolbox by considering the nodes as active species in templates.

(CSTR) enabled the programmable construction of an *in vitro* oscillating CRN in a defined environment.[17] The dynamics of such systems can be further tuned by considering shared resource usage and negative autoregulation to match output and demand.[18,19] Establishing predefined dynamic behaviors has also been achieved with enzymatically enriched RNA and DNA-based biochemical reactions based on transcription and replication.[20,21] Recent work has revealed that interconnecting DNA templates (or genelets) with RNA transcripts as dynamical species can yield switches,[22,23] oscillators,[24,25] and adaptation.[26] The successful compartmentalization of these dissipative biochemical reaction networks in water-in-oil microdroplets is further paving the way toward the design of artificial cells capable of molecular communication with living cells or other protocells.[27−29] Networks that are based on DNA replication, nicking, and degradation (*i.e.*, the PEN toolbox) can show stable oscillations,[30] multistability,[31] traveling waves,[32,33] symbiosis, and chaotic dynamics,[34] further demonstrating the bottom-up programmability of fundamentally different types of network topologies. Indeed, the reactions of this PEN toolbox are computationally[35] and experimentally well characterized,[36] making the toolbox an excellent choice to study and design new types of network topologies and their associated dynamics.

Here, we focus on systematic bottom-up design of CRNs employing the PEN toolbox. We report the automated design of biochemical networks constructed from the PEN toolbox displaying predefined dynamics. Specifically, an *in silico* approach is presented in which the multidimensional parameter space of dynamical models representing two key network motifs is explored, resulting in parameter regions in which the molecular circuits show either sustained oscillations or adaptation.[37−40] Next, the robustness to perturbations in the parameters of each circuit is assessed. By selecting the most robust parameter set, the chance of successful *in vitro* implementation is further increased. The information that is obtained from this computational analysis is subsequently used to automatically design optimal DNA sequences having hybridization energies that closely adhere to the design criteria as obtained from the robustness analysis. We perform this procedure on a network topology capable of oscillatory dynamics (the Oligator[30]) and on a PEN implementation of a type-1 incoherent feedforward loop (IFFL),[41] which is shown

dx.doi.org/10.1021/sb500300d | *ACS Synth. Biol.* XXXX, XXX, XXX−XXX

to display adaptation.[40] Finally, we reveal and characterize a previously unexplored reaction in the degradation kinetics of the components caused by unproductive sequestration of exonuclease by phosphorothioate modified ssDNA strands. Through simulation and mathematical analysis we demonstrate that the additional load on the degradation machinery results in an efficient amplification mechanism that increases the sensitivity of the computed adaptive response and enhances the robustness of the circuit under parametric uncertainty.

RESULTS AND DISCUSSION

Automated Design of Programmable PEN Toolbox Networks. The PEN toolbox is based on two fundamental types of reactions as building blocks, that is, activation (Figure 1A) and inhibition (Figure 1B). These reactions are triggered by short ssDNA strands, which act as regulating signals on longer ssDNA templates resulting in production of an output signal. Activation of templates by short ssDNA input strands enables DNA polymerase to extend the oligomer−template pair resulting in fully hybridized dsDNA strands, which are subsequently nicked resulting in double-stranded complexes consisting of templates, input strands, and newly synthesized output strands. Because reactions are performed at temperatures close to the melting temperature of the partial duplexes, input and output strands readily dissociate from their templates. Templates are inhibited by ssDNA strands that are complementary to part of the template's sequence but lack a nickase recognition site. An inhibitor further possesses a two-base mismatch at its 3′ end, preventing extension of the partial duplex thus rendering the template strand inactive. Signal and inhibition strands are degraded over time by exonucleases, while each template strand is protected against degradation by means of phosphorothioate modifications at its 5′ end. Figure 2A provides an overview of all types of reactions that occur in the PEN toolbox with respect to a single DNA template *T*. Because each template strand in a PEN derived CRN is equivalent to a functional node in a network motif, the regulation of a template's activity by another template through a signal ssDNA is equivalent to an edge in a network motif. Using this approach, the PEN toolbox can be used as a versatile tool to design network topologies capable of oscillatory (Figure 1C) or adaptive (Figure 1D) behavior. The temporal behavior of such a system is described by ordinary differential equations (ODEs) corresponding to the reactions. An arbitrary network topology is implemented with the PEN toolbox by correctly attributing the exact functionality of oligomers α, β, and *inh* with respect to other templates.

The first two crucial steps of the *in silico* design approach (Figure 2B) are selecting a network topology that is known to display a specific dynamic behavior followed by generating the set of ODEs. The set of ODEs is then used to guide circuit design by characterizing the functional parameter space corresponding to the desired behavior (Supporting Information Text S1). This characterization is performed by randomly generating key parameters of the system within certain ranges, that is, the initial concentrations of DNA templates and trigger strands (*vide infra*), and the hybridization dissociation constants that are tunable via changes in the base sequence. In this work, we have kept the Michaelis−Menten parameters and concentrations of exonuclease, nickase, and polymerase constant at previously determined literature values.[31] Although the concentrations of the three enzymes could be varied *in silico*, an incomplete mechanistic understanding of the

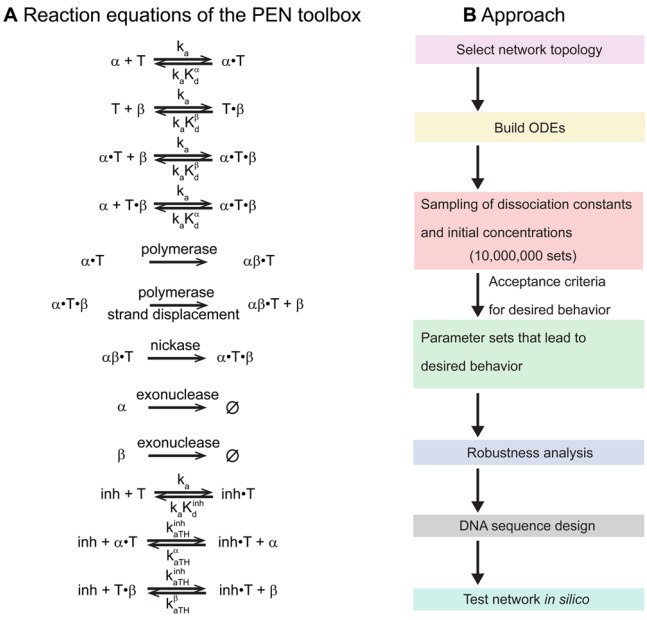

Figure 2. *In silico* design of *in vitro* biochemical reaction networks using the polymerase-exonuclease-nickase (PEN) toolbox. (A) Reaction equations of the PEN toolbox. The forward rate constant of hybridization k_a is assumed to be sequence independent[43] and fixed at a previously determined value of 0.06 nM^{-1} min^{-1}.[31] The backward rate constant of hybridization is expressed as the product of the forward rate constant k_a and the equilibrium dissociation constant K_d. The forward rate constant of inhibitor binding to an occupied template, $\alpha{\cdot}T$ or $T{\cdot}\beta$, via a toehold, k^{inh}_{aTH}, is chosen equal to k_a, because the toehold length is 6 or 7 bases. The forward rate constants k^{α}_{aTH} and k^{β}_{aTH} are lower, because they initiate strand displacement reactions via shorter toeholds of 3 bases. See Supporting Information Text S1 for details. Polymerase, nickase, and exonuclease activities are described assuming Michaelis−Menten kinetics. (B) The *in silico* approach. First, the ODEs for the network are derived, and subsequently, sampling all dissociation constants K_d and relevant initial concentrations between realistic values (*e.g.*, 10 million randomly generated sets) is then used to optimally cover the parameter space of the model. The K_d values correspond to hybridization energies, ΔG°_{AB}, that are matched by choosing the correct base sequence (Supporting Information Text S2). Responses of the network that meet certain criteria are accepted and analyzed further. The corresponding parameter sets are subjected to robustness analysis, and the parameter set that is characterized as most robust is used as a target for the DNA sequence design algorithm. Thermodynamic parameters obtained from the DNA sequence design algorithm will slightly deviate from the optimal set found using robustness analysis, and therefore, the network is simulated *in silico* again to validate the response.

isothermal amplification of partial duplexes by extension and nicking precludes the formation of a detailed kinetic model.[44] Therefore, the dissociation constants and the concentrations are the model parameters that are translated to experimental parameters.

Generally, the desired dynamic behavior is observed for a subset of the sampled parameter sets, called viable sets. The robustness of each of these viable sets is quantified in terms of a robustness measure (Supporting Information Text S2),[45,46] and the set that exhibits the highest robustness is used as the target set for the automated DNA strand design algorithm (*vide infra*).

We demonstrate the methodology on a network motif that has been previously shown to display oscillatory dynamics, the Oligator, corresponding to the left topology in Figure 1C.[30]

dx.doi.org/10.1021/sb500300d | *ACS Synth. Biol.* XXXX, XXX, XXX−XXX

Figure 3A depicts the reaction scheme of the Oligator. Template T_1 serves as an autocatalytic module that produces

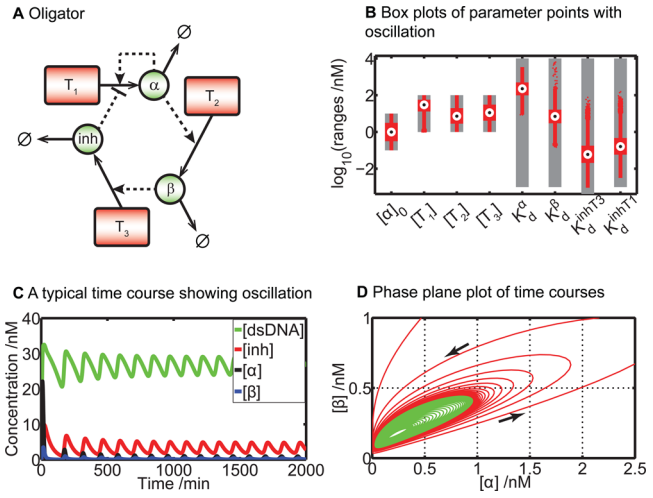

Figure 3. Design of a biochemical oscillator using the PEN toolbox. (A) Network topology of the Oligator as implemented by the PEN toolbox.[30] (B) Box plots of parameter points with oscillation. The gray bars indicate the sampling ranges for each parameter, and the red box plots correspond to parameter values leading to sustained oscillations. Notably, the median of template T_2 is lower than that of T_1 and T_3, indicating that high concentrations of template T_2 tend to destroy oscillatory behavior, because the delay time becomes insufficiently short. Furthermore, oscillatory behavior is also critically dependent on strong inhibition of T_1. (C) A typical oscillatory response of the Oligator, showing trajectories of the total dsDNA concentration, and the individual signal oligomers *inh*, α, and β. For this system, sampling resulted in K_d^{α} = 127 nM, K_d^{β} = 3.7 nM, K_d^{inhT3} = 0.63 nM, K_d^{inhT1} = 0.9 nM, $[\alpha]_0$ = 5 nM, $[T_1]$ = 16 nM, $[T_2]$ = 3 nM, and $[T_3]$ = 16 nM. (D) Trajectories plotted in the $[\alpha]$-versus-$[\beta]$ plane. Numerically, there is a single limit cycle that attracts all trajectories. The red trajectory is the response shown in C where the amplitudes of the oscillations decrease toward the limit cycle. The green trajectory results from initial conditions close to the equilibrium and shows oscillations of increasing amplitude converging toward the limit cycle.

oligomer α while reactions on template T_2 result in a delay in the activation of T_3 via ssDNA oligomer β. The product of T_3, oligomer *inh*, in turn, inhibits the autocatalytic activity of T_1. Box plots corresponding to the functional parameter space leading to an oscillatory response are depicted in Figure 3B, and the sampling ranges are indicated by bars.[47] Cross-correlations between the sampled parameters are displayed in Supporting Information Figure S2. From the box plots, it is observed that the optimal concentration of template T_2 is significantly lower than the optimal concentrations of templates T_1 and T_3, suggesting that high concentrations of template T_2 tend to destroy oscillatory behavior. This trend is supported by the original experiments[30] and can be rationalized by the fact that high concentrations of T_2 results in rapid production of inhibitor via template T_3, which makes the time-delay over the negative feedback loop too short. Importantly, once the inhibitor is formed, it should strongly inhibit T_1 (low value of K_d^{inhT1}) as a fast shutdown of the positive feedback loop is necessary to generate sustained oscillations. Finally, the delicate balance between contributions from the positive and negative feedback loop in the Oligator becomes apparent from the optimal median value of K_d^{α}. Sustained oscillations only appear if oligomer α rapidly dissociates from templates T_1 and T_2 (*i.e.*, K_d^{α} adopts high values). We attribute this to the fact that rapid dissociation of oligomer α prevents saturation of template T_1, and hence, a fast exponential increase of α is guaranteed. On the other hand, fast dissociation of α from T_2 also contributes to the increased time-delay over the negative feedback loop. A typical oscillatory response is depicted in Figure 3C where the total base-pair concentration is shown as a function of time, along with the temporal concentration profiles of the individual oligomers α, β, and *inh*. We verify that there is a single limit periodic trajectory in Figure 3D in the $[\alpha]$-versus-$[\beta]$-plane and that, regardless of the initial condition, the response spirals toward that same trajectory. Our *in silico* analysis of the Oligator CRN is thus able to identify ranges of thermodynamic parameters and template concentrations that give rise to oscillatory responses and thus greatly facilitates successful experimental implementation. Moreover, these results corroborate with experimental findings by Rondelez and co-workers.[30]

The procedure is repeated to investigate if a PEN implementation of a type-1 IFFL (Figure 4A) is able to display adaptation. Adaptation is the ability of a system to respond to a change in stimulus after which it returns to prestimulus activity while the stimulus level stays elevated. Sensitivity and precision are measures for the relative response to change in stimulus and the relative difference in steady state values, respectively, and are defined in eq 1 related to the signal in Figure 4B.

$$S = \left| \frac{(Y_p - Y_1)/Y_1}{(U_2 - U_1)/U_1} \right|, \qquad P = \left| \frac{(Y_2 - Y_1)/Y_1}{(U_2 - U_1)/U_1} \right|^{-1} \tag{1}$$

We have chosen the type-1 IFFL because previous work has shown that this pulse-generating motif can control gene expression *in vivo*,[48] and adaptation in type-1 IFFL network motifs is more robust compared to adaptation arising in NFBLB network motifs *in silico*.[40] Furthermore, alternative implementations of DNA based IFFL circuits show adaptive responses of similar quality compared to the circuit shown in Figure 4A (Supporting Information Text S1); however, the concentration of output ssDNA is lower. In the type-1 IFFL circuit considered here, activation occurs on template T_1 by input strand U that is resistant to degradation. Activation of T_1 by U initiates production of oligomer α that in turn activates both T_2 and T_3. Activation of T_3 leads to the production of output oligomer Y, while activation of T_2 leads to the production of inhibitor *inh*, which renders T_3 inactive. To explore the phase space of this circuit, simulations were performed in which the system is first equilibrated and the response in the concentration of free Y to a doubling of the concentration of U is evaluated. The response of the network measured by the concentration of free Y is classified as adaptive if the sensitivity (S) and precision (P) exceed preset threshold values, that is, $\log_{10}(S) > -0.5$ and $\log_{10}(P) > 1$ (Figure 4B). Figure 4C shows box plots that indicate ranges in the concentration and hybridization constants for which the IFFL circuit is able to display an adaptive response. Cross-correlations between the sampled parameters are displayed in Supporting Information Figure S4. The IFFL circuit displays adaptive dynamics when the hybridization dissociation constants of oligomers α and Y to their respective templates are high compared to the other hybridization constants, reflecting the fact that fast activation of T_2 and T_3 ensures rapid synthesis of free Y. The low affinity of output Y for T_3 prevents sequestration of Y by its template, which is critical to achieve a response with a high sensitivity. In order for the

dx.doi.org/10.1021/sb500300d | ACS Synth. Biol. XXXX, XXX, XXX−XXX

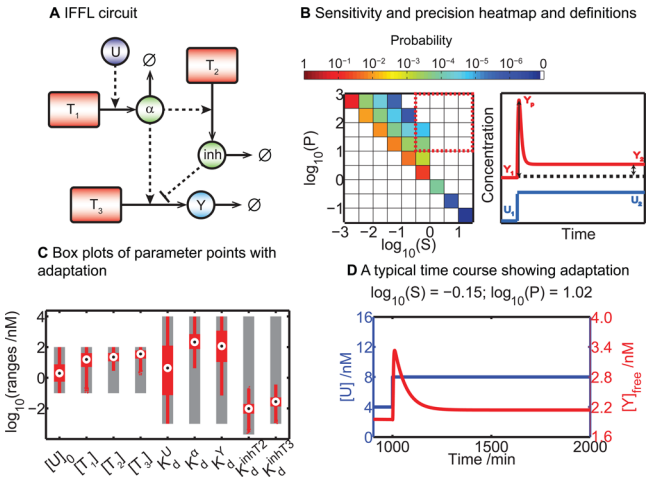

Figure 4. Design of an adaptive biochemical circuit using the PEN toolbox. (A) Network topology of a PEN-toolbox implementation of a type-1 incoherent IFFL. Input trigger U is protected from degradation by exonuclease through multiple phosphorothioate modifications at the 5′ end of its backbone. To characterize the effect of these backbone modifications on the kinetics of DNA polymerase when U acts as the trigger on T_1, we experimentally determined $V_{max,polU}$ and $K_{M,polU}$ and used these in the model (Supporting Information Text S4, Figure S13). (B) Heatmap of the probability of finding a certain combination of sensitivity and precision values, along with the definitions of sensitivity and precision. The adaptive regime ($\log(S) > -0.5$ and $\log_{10}(P) > 1$) is highlighted by a red dashed box. Notably, the probability of finding an adaptive response through sampling is low (hit rate is 0.05%). In the signal, the characteristic measures that determine sensitivity and precision (eq 1) are displayed. (C) Box plots as a result of parameter sampling of the IFFL motif. The gray bars indicate the sampling ranges for each parameter, and the red box plots correspond to parameter values leading to adaptation. The analysis shows that the concentrations of input oligomer U and templates T_1, T_2, and T_3 can be tuned such that the network displays an adaptive response in the concentration of free Y. The dissociation constants for oligomers α and Y are near their upper sampling bounds, which is explained by the need for fast activation of T_2 and T_3 ensuring rapid synthesis of output Y. The low affinity of Y for T_3 prevents sequestration of Y by its template. In order to overcome the transient increase in Y, that is, matching the steady state value of Y after the transient increase to the previous steady state as closely as possible and thus maximizing the precision of the response, inhibition of T_3 must be very strong. This explains the low values found for dissociation constant K_d^{inhT3} (and hence also K_d^{inhT2}). The concentration of T_3 is high because the response in Y must be noticeable when inhibition is strong. (D) Adaptation as observed in the concentration of oligomer Y in its free form. The parameters corresponding to this response are $K_d^U = 14.6 \times 10^3$ nM, $K_d^\alpha = 1.8 \times 10^3$ nM, $K_d^{inhT2} = 0.037$ nM, $K_d^Y = 5.8 \times 10^3$ nM, $K_d^{inhT3} = 0.042$ nM, $[U]_0 = 4$ nM, $[T_1] = 24$ nM, $[T_2] = 12$ nM, and $[T_3] = 95$ nM.

adaptive response to display a high precision, that is, the free concentration of Y returns to prestimulus levels, inhibition of T_3 by *inh* must be very strong, which is reflected in low values of the dissociation constant K_d^{inhT3} (and K_d^{inhT2}). The concentration of template T_3 adopts a high value because the response in Y must be noticeable even though inhibition is strong. The heatmap in Figure 4B depicts the probability of finding a response with a certain sensitivity and precision. An important observation from this heatmap is that $\log_{10}(S)$ does not exceed the value 0 (or S does not exceed 1), indicating fold changes in the transient response in Y is unable to exceed fold-changes in the concentration of input U. The automated circuit design is able to identify an adaptive responses in the DNA-based IFFL (Figure 4D), however; the sensitivity of the network is always lower than one (*vide infra*). Hence, we have shown using two distinct network topologies that an automated approach is successful in finding functional dynamical behavior in DNA-based enzymatic CRNs.

Robustness Analysis and Automated DNA Sequence Design. *In silico* design of synthetic biochemical circuits consists of a performance and a robustness classification phase.[52] In the previous sections, we have classified the performance of two DNA-based CRNs resulting in parameter ranges where the desired response can be observed. However, this procedure does not yield insight in the robustness of the response, that is, the effect of small perturbations on the performance of the circuit. We have used the "glocal" robustness concept as introduced by Wagner et al. to compute a robustness measure for each dissociation constant for the two PEN-based circuits (Figures 3A and 4A) and have used this information in the design of template sequences.[45] Because the number of viable parameter sets resulting in the desired dynamical behavior is small for both circuits (0.05−0.3%), we first vastly increased the number of viable parameter sets by a directed parameter search of the parameter space close to the viable sets (Supporting Information Text S2, Figure 5A). All resulting parameter sets are locally perturbed, leading to a robustness measure for each parameter set. Next, the dissociation constants of the set with the highest robustness measure are perturbed individually such that every dissociation constant in the circuit is associated with an individual robustness measure between 0 and 1 (Supporting Information Figures S7 and S8). The robustness measure for each hybridization dissociation constant is used as a weighting factor in the automated DNA strand design procedure (Supporting Information Text S3, Figure 5B). The hybridization Gibbs free energy values are calculated from the optimal dissociation constants and are subsequently used as target Gibbs free energies for automated DNA sequence design. A simulated annealing approach[53] is used to perform the sequence optimization. In this process, we suggest point mutations in the DNA strands, calculate the DNA hybridization Gibbs free energies using NUPACK[50,51] and evaluate the value of the objective function. The objective function is based on the weighted error between the target and calculated Gibbs free energy values of DNA hybridizations and contains penalties for intramolecular hybridization of ssDNA strands and unintended cross-hybridizations between the various components of each network topology. Unique DNA sequences are generated using the criton[54] concept introduced by Seeman (Supporting Information Text S3). Eventually, the Gibbs free energy values converge toward their respective target values. For the IFFL motif, this convergence is shown for the duplexes $T_1{\cdot}\alpha$, $T_3{\cdot}Y$, and $inh{\cdot}T_3$ in Figure 5C. The iteration that displays the minimum total error corresponds to the sequences of choice for *in vitro* characterization. The DNA sequences resulting from the optimization procedure, with the necessary modifications to retain functionality of the circuit, are depicted in Table 1.

Unproductive Sequestration of ttRecJ Exonuclease. During experimental characterization of the PEN toolbox, we discovered that ttRecJ exonuclease binds strongly to phosphorothioate protected ssDNA strands thereby preventing binding of degradable unprotected ssDNA strands (Figure 6A). We believe that this binding is the result of strong metal−ligand interactions between sulfur atoms on the modified DNA

dx.doi.org/10.1021/sb500300d | ACS Synth. Biol. XXXX, XXX, XXX−XXX

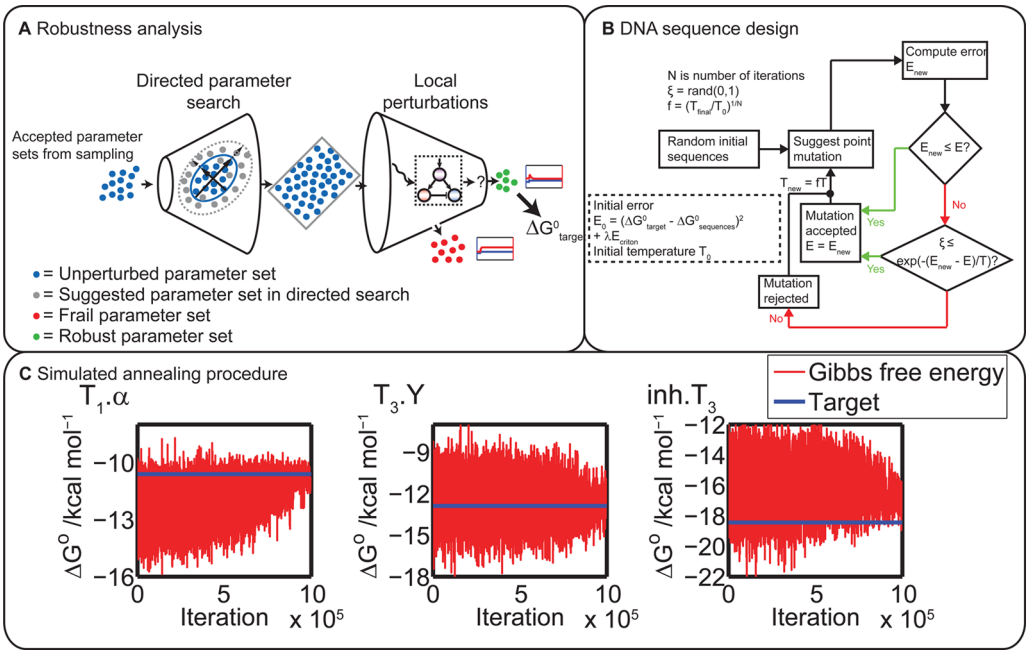

Figure 5. Parameter robustness analysis and automated DNA sequence design. (A) Schematic representation of the parameter robustness analysis procedure. From the sampling, accepted parameter sets that generate the desired dynamic network behavior are subjected to a directed parameter search vastly increasing the number of viable sets.[45] Once this procedure has converged, all resulting sets are locally perturbed, resulting in a robustness measure for each parameter set. The most robust parameter set is then taken and used as a target for DNA sequence design. (B) Simulated annealing procedure for automated DNA sequence design.[49] The parameters resulting from the robustness analysis are used to calculate the optimal Gibbs free energy of DNA hybridization, and these are subsequently used as target Gibbs free energies for automated DNA sequence design. DNA hybridization Gibbs free energies are calculated by NUPACK[50,51] and should match the targets as closely as possible. Next to optimization of the Gibbs free energies of hybridization, self-complementarity and unwanted inter- and intramolecular hybridization is penalized. Therefore, this approach provides optimal DNA hybridization energies while minimizing circuit leakage due to undesired enzymatic reactions. (C) Gibbs free energy convergence by means of simulated annealing to the target values as determined for the IFFL circuit network to show adaptation, shown for the duplexes $T_1{\cdot}\alpha$, $T_3{\cdot}Y$, and $inh{\cdot}T_3$. A million point mutations are performed, and the iteration showing the lowest total error corresponds to the DNA sequences that can be used to experimentally implement the network.

Table 1. DNA Sequences for the IFFL Circuit Resulting from the Automated Design[a]

oligomer	sequence
T_1	A*T*T*A*GACTC*ACAAACGACTCCTA*
T_1*	A*T*T*A*GACUC*ACAAACGACTCCTA*
T_2	A*T*C*CCAACATTAGACTATTA*GACTCAC*
T_3	A*A*A***TA**CCCAACATTA*GACTCAC*
U	T*A*G*GAGTCGTTT
α	GTGAGTCTAAT
Y	GTTGGGTATTT
inh	AGTCTAATGTTGGG**AT**

[a]Marked bases (*) are protected from degradation by exonuclease through phosphorothioate modifications on their 5′ backbones. Italic bases belong to the nickase recognition sites, bold bases belong to the imposed 2-base mismatch of the inhibitor strand on T_3. Sequences are depicted 5′ → 3′. The nickase recognition site of template T_1 close to the phosphorothioate modifications is mutated (T_1*, thymine → uracil) in order to obtain a comparable nicking rate with respect to nickase recognition sites located at the 3′ end.[31]

backbone and Mn^{2+} or Mg^{2+} sites present in the exonuclease binding pocket.[55] This unproductive sequestration can result in unintentional cross-coupling between network components, and therefore, the dissociation constant (K_I) characterizing this binding event was quantified. Table 2 displays the dissociation constants of the protected oligomers T_1 and U as determined at 42 °C in master mix (Supporting Information Text S4). We find that the dissociation constant characterizing the competitive inhibition of exonuclease by protected ssDNA strands depends on the length of the DNA strand and find a higher affinity of ttRecJ for shorter protected strands (Supporting Information Figure S15).

Next, we investigated how unproductive sequestration of the degradation machinery by protected ssDNA strands influences the adaptive response of the DNA-based IFFL. Previous reports have quantified how resource competition coupled with enzyme saturation in genetic networks can lead to ultrasensitive responses,[56] allows for predictable tuning of bistable switches[57,58] and presents a versatile mechanism to synchronize and tune oscillating circuits.[59−62] However, the influence of resource competition on adaptation dynamics has, to the best of our knowledge, not been reported. We expanded the ODE model by explicitly taking into account unproductive binding of the ttRecJ exonuclease to protected ssDNA strands and assessed the ability of the improved model to display adaptation. In contrast to the model in which sequestration of exonuclease by protected ssDNA strands is neglected (Figure 4B), the response heatmap (Figure 6B) of the improved model shows that the circuit is capable of adaptive responses characterized by high sensitivity values ($\log_{10}(S) > 0$) while maintaining precision ($\log_{10}(P) > 1$), that is, output signals that return to prestimulus activity show a transient response exhibiting a sensitivity value larger than one. Mechanisms that lead to signal amplification in adaptation dynamics[63] of biological circuits include covalent modifications of receptors[64] by means of zeroth order ultrasensitivity[40,65] and

dx.doi.org/10.1021/sb500300d | ACS Synth. Biol. XXXX, XXX, XXX−XXX

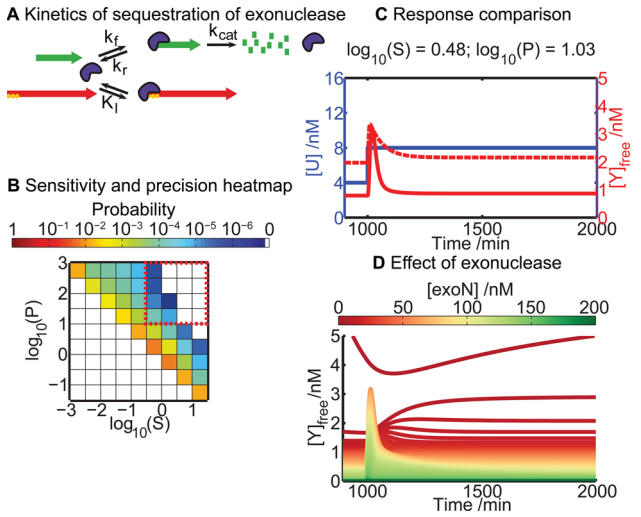

Figure 6. Unproductive sequestration of exonuclease. (A) Mechanism: exonuclease (purple) binds to ssDNA strands (green), which are subsequently degraded. However, the degradation of unprotected ssDNA oligomers is inhibited by binding of phosphorothioate protected (yellow circles) ssDNA oligomers (red) competing for the active site of the exonuclease. (B) Heatmap of the probability of finding a certain combination of sensitivity and precision values (10^7 samples). The adaptive regime ($\log_{10}(S) > -0.5$ and $\log_{10}(P) > 1$) is highlighted by a red dashed box. Notably, responses that exhibit sensitivity values larger than 1 ($\log_{10}(S) > 0$) while maintaining precision are found. (C) Comparison of an adaptive response without (dashed lines, Figure 4D) and with (solid lines) competitive inhibition of exonuclease by phosphorothioate protected strands. Competitive inhibition of the degradation machinery results in an amplified adaptive response characterized by sensitivity larger than 1. The parameters corresponding to this response are $K_d^U = 14.6$ nM, $K_d^\alpha = 1.8 \times 10^3$ nM, $K_d^{inhT2} = 0.037$ nM, $K_d^Y = 5.8 \times 10^3$ nM, $K_d^{inhT3} = 0.042$ nM, $[U]_0 = 4$ nM, $[T_1] = 24$ nM, $[T_2] = 12$ nM, $[T_3] = 95$ nM, and $[exoN] \approx 50$ nM. The lower steady state for the improved model is explained by less availability of DNA templates due to unproductive sequestration. (D) Effect of the exonuclease concentration in the model that incorporates competitive inhibition of exonuclease with the same parameters as in C. A concentration of $[exoN] \approx 50$ nM exhibits the best response. Very high exonuclease concentrations lead to extremely low ssDNA concentrations and no significant response in Y.

Table 2. Dissociation Constants Quantifying Unproductive Binding of Protected ssDNA Strands to Exonuclease ttRecJ[a]

oligonucleotide	K_I (nM)
U (12 bases)	1.38 ± 0.02
T_1 (23 bases)	4.72 ± 0.01

[a]Dissociation constants were determined at 42 °C in master mix using three different sequences of oligomer T_1 and U carrying three phosphorothioate modifications (Supporting Information Text S4, Figure S15). The table depicts the mean dissociation constants obtained by analysis of several variants of oligomer U and T_1. The $V_{max,exoN}$ and $K_{M,exoNlong}$ that describe degradation of oligomer *inh* in absence of protected competitors is obtained from nonlinear least square analysis of the data using the integrated Michaelis–Menten equation without competition ($V_{max,exoN} = 169.97 \pm 1.80$ nM min^{-1} and $K_{M,exoNlong} = 529.76 \pm 17.43$ nM).

receptor clustering.[66] Importantly, none of these mechanisms plays a role in the DNA-based IFFL circuit. Figure 6C shows a response of the improved model exhibiting amplified exact adaptation ($\log_{10}(S) > 0$ and $\log_{10}(P) > 1$) alongside a response of the original circuit with the same parameters as in Figure 4D.

Figure 6D displays the effect of the concentration of exonuclease on the quality of the response. Low availability of exonuclease leads to accumulation of ssDNA strands, saturating the templates, thus reducing the relative responses of the system. As the exonuclease concentration increases, the response time and steady state concentration of Y decrease, while the peak value stays approximately constant, thus increasing sensitivity. The concentration of exonuclease reaches an optimal point at which the system displays its optimal response, after which further increase decreases the overall quality of the response because ssDNA strands are degraded too fast. Near the optimal exonuclease concentration, the nonlinearity introduced by high affinity of the enzyme for protected ssDNA allow these strands to function as a buffer for enzymatic activity, which is necessary for the circuit to exhibit $S > 1$. Moreover, the parameter regimes in which exact adaptation ($\log_{10}(S) > -0.5$ and $\log_{10}(P) > 1$) occurs are significantly broadened due to unproductive exonuclease sequestration (Supporting Information Figure S16), while the robustness measures of the parameters increase (Supporting Information Figure S17). From this, we can conclude that unproductive sequestration of the degradation machinery of the DNA-based IFFL circuit appears to greatly improve the quality and robustness of the adaptive response.

The origin of this behavior can be unraveled through modeling. The ODE models presented earlier are kinetically detailed and provide stringent criteria for DNA sequence design, but they are too complex to enable a conceptual understanding of the nonlinear dynamics underlying the adaptation mechanism. To that end, we constructed two toy models lacking detailed kinetics but allowing one to explore and rationalize qualitative behavior. The first toy model (TMI) is a compact representation of the original design of the IFFL circuit, whereas the second one (TMII) additionally includes additional resource competition by unproductive sequestration of the protected, nondegradable input strand by exonuclease. It should be noted that the three-node networks analyzed by Tang and co-workers[40]—contrary to our three-node circuits—are based on reactions that describe enzymatic conversions from a conserved pool, that is, each node of the circuit relates to a constant total concentration of enzyme that is interconverted between an active and an inactive form. The simplified ODE models analyzed in this paper are fundamentally different as the interacting species α, *inh*, and Y are constantly produced (by polymerase from dNTPs) and degraded (by exonuclease) over time. TMI is described in eqs 2–4, where the production of the activator (α), inhibitor (*inh*), and output (Y) is modeled by Michaelis–Menten kinetics and their degradation by first-order kinetics (*vide infra*).[31,34]

$$\frac{d\alpha}{dt} = \frac{k_\alpha T_1 U}{K_U\left(1 + \frac{U}{K_U}\right)} - D\alpha \tag{2}$$

$$\frac{dinh}{dt} = \frac{k_{inh} T_2 \alpha}{K_\alpha\left(1 + \frac{\alpha}{K_\alpha}\right)} - Dinh \tag{3}$$

$$\frac{dY}{dt} = \frac{k_Y T_3 \alpha}{K_\alpha\left(1 + \frac{\alpha}{K_\alpha} + \frac{inh}{K_{inh}}\right)} - DY \tag{4}$$

dx.doi.org/10.1021/sb500300d | ACS Synth. Biol. XXXX, XXX, XXX–XXX

In these equations, U represents the total concentration of input strand, whereas α, *inh*, and Y are the concentrations of the activating, inhibiting, and output species in the IFFL circuit. T_1, T_2, and T_3 are the concentrations of the template strands, while the parameters K_U, K_α, and K_{inh} are Michaelis–Menten constants—roughly equal to the hybridization dissociation constants K_d^U, K_d^α, and $K_d^{inhT2} \approx K_d^{inhT3}$ in the large ODE model, respectively. The rate constants k_α, k_{inh}, and k_Y are catalytic rates depending nontrivially on nickase and polymerase enzyme kinetics, while D represents the first-order degradation rate constant. In principle, competition between the network constituents for exonuclease should result in nonlinear degradation terms. However, the first-order approximation remains valid, as the individual concentration of each of these species is well below the Michaelis–Menten constant of exonuclease for unprotected strands ($K_{M,exoN} \sim 150–440$ nM). Inhibition of T_3 by *inh* is taken into account by assuming that this species acts as a competitive inhibitor cf. eq 4.

It can be readily shown that TMI exhibits high precision but the sensitivity of its adaptive response is below one (Supporting Information Text S5). This is in excellent agreement with our earlier observation that the DNA-based enzymatic IFFL circuit fails to amplify transient changes in its input. Intuitively, the output dynamics of TMI are characterized by the total concentration of input strand. For low total concentrations of input, the enzyme kinetics in eqs 2–4 operate in their linear regime, whereas high concentrations saturate it. The inhibitory effect of *inh* on Y is negligible in the former case, resulting in a steady state value $\overline{Y}$ of the output that grows roughly proportionally with U; that is, the network is imprecise. In the latter case, *inh* inhibits the output successfully, making $\overline{Y}$ largely insensitive to changes in U, that is, the network exhibits high precision. This becomes obvious from the explicit formula for the steady state (eq 5)

$$\overline{Y} = \overline{Y}_{max}\frac{U^2 + KU}{U^2 + K'U + K''} \tag{5}$$

which yields the approximations $\overline{Y} \approx \frac{K\overline{Y}_{max}}{K''}U$ and $\overline{Y} \approx \overline{Y}_{max}$ for low and high concentrations U, respectively. The expressions for the constants K, K', and $K''$are given in Supporting Information Text S5. Summarizing, while TMI is able to generate adaptive responses with high precision, the sensitivity of the response is low ($S < 1$).

The second toy model, TMII, is a modification of TMI incorporating the observation that protected species are able to unproductively bind exonuclease (*exoN*), which results in enzyme-limited competition. Here, we only consider the binding between input strands and exonuclease, neglecting binding of protected templates. This is in agreement with TMI, where changes in template concentrations were unaccounted. Specifically, we incorporate unproductive sequestration by introducing competition between exonuclease and template T_1 for protected input strand (mechanism is depicted in eq 6).

$$U + exoN \underset{k_{r,exoN}}{\overset{k_{f,exoN}}{\rightleftharpoons}} U{\cdot}exoN, \qquad K_{I,U} = \frac{k_{r,exoN}}{k_{f,exoN}}$$

$$U + T_1 \underset{k_{d,U}}{\overset{k_a}{\rightleftharpoons}} U{\cdot}T_1, \qquad K_d^U = K_U = \frac{k_{d,U}}{k_a} \tag{6}$$

TMII uses the free concentration of input strand, that is, $U_{free} = U - U{\cdot}exoN - U{\cdot}T_1$, as a competitive inhibitor in the degradation terms. Amplification of α by T_1 is also initiated by the free form of input ssDNA; hence, TMII is described as in eqs 7–9. We again note the difference to the simplified ODE models analyzed by Tang and colleagues,[40] as in TMII the input explicitly affects network dynamics by controlling the degradation rates due to sequestration of exonuclease activity.

$$\frac{d\alpha}{dt} = \frac{k_\alpha T_{1,tot} U_{free}}{K_U\left(1 + \frac{U_{free}}{K_U}\right)} - \frac{V_{max,exoN}\alpha}{K_{M,exoN}\left(1 + \frac{U_{free}}{K_{I,U}}\right)} \tag{7}$$

$$\frac{dinh}{dt} = \frac{k_{inh} T_2 \alpha}{K_\alpha\left(1 + \frac{\alpha}{K_\alpha}\right)} - \frac{V_{max,exoN} inh}{K_{M,exoN}\left(1 + \frac{U_{free}}{K_{I,U}}\right)} \tag{8}$$

$$\frac{dY}{dt} = \frac{k_Y T_3 \alpha}{K_\alpha\left(1 + \frac{\alpha}{K_\alpha} + \frac{inh}{K_{inh}}\right)} - \frac{V_{max,exoN} Y}{K_{M,exoN}\left(1 + \frac{U_{free}}{K_{I,U}}\right)} \tag{9}$$

In these equations, $V_{max,exoN}$ is the maximum degradation rate and $K_{M,exoN}$ is the Michaelis–Menten constant of exonuclease, while $K_{I,U}$ is the dissociation constant of protected U unproductively binding to exonuclease. Sequestration is assumed to occur instantaneously; that is, U_{free} is obtained at each time-step by solving the algebraic equations corresponding to the steady state of eq 6.

TMII displays an adaptive response with high precision under the same conditions as TMI. The mechanism enabling adaptation is similar to that in TMI, with the steady state values of the model components behaving differently for input strand concentration in excess of $U > exoN + T_1$ (Figure 7B). In contrast to TMI, however, TMII is capable of generating adaptive responses with high sensitivity for input concentrations around $U \approx exoN + T_1$ (Figure 7A). Amplified exact adaptation in TMII is driven by unproductive binding of input strand to exonuclease, as a result of large relative decreases in the degradation rates for $U \approx exoN + T_1$ (Figure 7C, bottom graph). To investigate this mechanism in detail, we first outline two operational modes for the circuit specified by the total concentration U relative to the summed concentration $exoN + T_1$. First, for concentrations $U < exoN + T_1$, most of the input is bound to exonuclease or template T_1 (Figure 7B), while the remainder drives the production of α, *inh*, and Y. In this mode, the steady state $\overline{Y}$ increases with the concentration U, similar to the linear regime in TMI. When $U > exoN + T_1$, exonuclease and template T_1 are nearly saturated and $U_{free} \approx U - exoN - T_1$. In this operational mode, the production terms are also saturated, and the inhibitory connection controls $\overline{Y}$ effectively (Supporting Information Text S5). In the regime intermediate to those modes, $U \approx exoN + T_1$, exonuclease and template T_1 approach saturation allowing $U_{free} \ll U$ to increase sharply with U (Figure 7B, bottom panel). This increase in U_{free} increases production rates and decreases degradation rates by unproductive sequestration of exonuclease, thereby elevating $\overline{\alpha}$, $\overline{inh}$, and $\overline{Y}$ sharply (Figure 7B, top two graphs). Precision increases rapidly in this transitory regime (Figure 7C, top panel), as $\overline{inh}$ arrests further production of $\overline{Y}$. Concurrently, changes in U affect U_{free} commensurately ($\delta U_{free} \approx \delta U$), but relative changes $\delta U_{free}/U_{free} \approx (U/U_{free})(\delta U/U)$ are starkly amplified by the factor $(U/U_{free}) \gg 1$ (Figure 7C, bottom graph). Such relative changes in U_{free} instantly affect the degradation rate, while the production machinery of Y responds much slower. The net result is a transient imbalance in the production and

dx.doi.org/10.1021/sb500300d | ACS Synth. Biol. XXXX, XXX, XXX–XXX

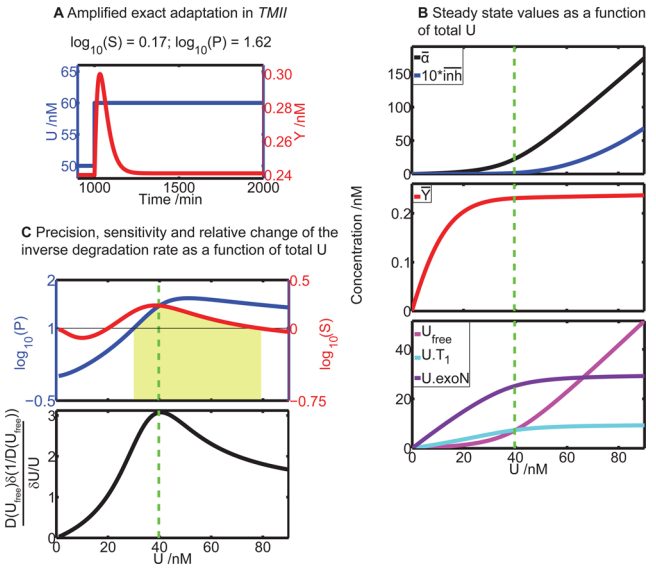

Figure 7. Analysis of TMII. (A) Amplified exact adaptation in TMII as a result of increasing the total concentration of input ssDNA by 20%. Parameter values for this simulation are K_U = 0.2 nM, K_α = 1250 nM, K_{inh} = 0.001 nM, $K_{I,U}$ = 1.4 nM, $K_{M,exoN}$ = 440 nM, $k_\alpha T_{1,tot}$ = 2.5 nM min^{-1}, $k_{inh}T_2$ = 8 nM min^{-1}, $k_Y T_3$ = 106.5 nM min^{-1}, and $V_{max,exon}$ = 300 nM min^{-1}. (B) Steady state values of the three states in the model, that is, $\bar{\alpha}$, $\overline{inh}$, and $\bar{Y}$, as a function of the total concentration of input strand, U (top two panels); the effect on both U_{free} and $U{\cdot}T_1$ of unproductive binding of input strand U to template T_1 and exonuclease (bottom panel). The dashed green lines represent the summed concentration $exoN + T_1$. (C) The top graph shows the logarithm of precision (blue) and sensitivity (red) as a function of the total concentration of input strand, U, with the amplified exact adaptation regime highlighted in yellow ($\log_{10}(S) > 0$ and $\log_{10}(P) > 1$). The bottom graph displays the relative change in inverse degradation rate (Supporting Information Text S5); degradation slows down when this measure becomes large, therefore correlating very well with sensitivity.

degradation of output, which drives a substantial overshoot in the response of the circuit signaling high sensitivity values (Figure 7A).

Conclusion. In this paper, we have shown the successful automated design of CRNs constructed from the PEN toolbox. An important asset of this approach is that it couples a directed exploration of the phase space and calculated robustness measures of parameters to a physical implementation of the desired circuit that is optimized to account for unexpected perturbations. Indeed, this coupling ensures that the expected functionality of the circuit is preserved after optimization of the DNA sequences. The automated design methodology has shown to successfully reproduce the Oligator system and is applied to the design of a new type of PEN-based circuit, the IFFL. Although the experimental implementation of the IFFL circuit may seem straightforward at this point, initial scoping experiments have revealed that the use of fluorescent probes that transiently sequester ssDNA output Y leads to strong retroactivity effects that negatively influence adaptation dynamics making characterization of the circuit dynamics extremely challenging.[67] Currently, we are working on various strategies to attenuate retroactivity effects in PEN-based circuits. In the future, the design procedure will be facilitated by the incorporation of automated generation of sets of ODEs, greatly speeding up the design process and reducing the risk of error-prone derivation of large sets of ODEs by hand. While the methodology is designed for reaction networks based on the PEN toolbox, similar approaches will alleviate the design of CRNs based on different building blocks, for example, those based on genelets or *in vitro* transcription−translation machinery, and the design of CRNs in microfluidic reactors. Next to the automated design of PEN-based circuits, we have characterized the unproductive sequestration of the degradation machinery of the PEN toolbox. The noncanonical cross-coupling between network components results in strong nonlinearities in their degradation, which can either suppress or promote target dynamic behavior.[60] For the case of the IFFL circuit, we have shown how noncanonical cross-coupling by enzyme-limited competition provides a novel amplification mechanism and broadens the parameter range in which the network displays adaptation. The results in this paper will aid in the development of integrated biochemical circuits that can probe their chemical environment, process chemical signals, make decisions, and take action at the molecular level.

METHODS

Integration of ODEs. All ODE computations are performed with MATLAB R2010a. Differential equations are numerically integrated with compiled MEX files using numerical integrators from the SUNDIALS CVode package.[68] The relative and absolute tolerances are always set to 10^{-11}, and a solution is required to be found within 10 s. Latin Hypercube Sampling is required to generate 10^7 parameter sets and is performed with scripts from Budiman Minasny (2004). See Supporting Information Texts S1 and S2 for more details.

DNA Sequence Design. A parser written in Python performs a simulated annealing procedure using point mutations in the DNA strands iteratively to design optimal DNA sequences. The parser is initiated by the user and communicates with the NUPACK executable complexes to obtain all relevant information needed to evaluate the binding energies of the DNA complexes, while the parser contains functions to evaluate DNA strand integrity based on the criton concept. Operational details of the parser and settings for NUPACK are described in Supporting Information Text S3.

Experimental Characterization of Polymerase and Exonuclease. Oligonucleotides were obtained from Integrated DNA Technologies (IDTDNA) and were purified using high performance liquid chromatography (HPLC). Three phosphorothioate backbone modifications at the 5′ end prevent degradation of templates and input primer U of the enzymatic DNA based network. Furthermore, templates were ordered with a phosphate modification at their 3′ end to prevent circuit leakage. Concentrations of DNA were verified using NanoDrop Spectrophotometer ND-100.

Enzymatic degradation of nonprotected primers is induced by ttRecJ, a thermophilic equivalent of the 5′ → 3′ processive exonuclease RecJ enzyme from *Thermus thermophilus*. The batch was diluted in diluent D (NEB) to form a stock solution with a concentration of 2.5 μM.

DNA polymerase was obtained from NEB. The working stock of Bst. polymerase was prepared by dissolving the original stock of 8000 U mL^{-1} in diluent A complemented with 0.1% Triton X-100 to form a stock of 256 U mL^{-1} (36.2 nM).

Full experimental protocols and analyses are given in Supporting Information Text S4.

dx.doi.org/10.1021/sb500300d | *ACS Synth. Biol.* XXXX, XXX, XXX−XXX

■ ASSOCIATED CONTENT

Supporting Information

Full descriptions of the sampling procedure, differential equations, robustness analysis, DNA sequence design algorithm, toy models, and the corresponding figures and results. This material is available free of charge via the Internet at http://pubs.acs.org.

■ AUTHOR INFORMATION

Corresponding Author

*E-mail: t.f.a.d.greef@tue.nl.

Notes

The authors declare no competing financial interest.

■ ACKNOWLEDGMENTS

H.W.H.v.R., L.H.H.M., and T.F.A.d.G. acknowledge financial support from The Netherlands Organisation for Scientific Research (NWO): Graduate Programme 2010, ECHO-STIP No. 717.013.001, VENI Grant No. 722.012.0001, and Gravity program No. 024.001.035. The authors thank R. Masui for the kind gift of ttRecJ and H. Salis for publicly providing his Ribosome Binding Site calculator, which served as an example for how to build a NUPACK wrapper in Python. We are grateful to Y. A. Rodenburg for initial work on DNA sequence optimization algorithms, and to F. L. P. Sips and Y. J. W. Rozendaal for discussions and careful reading of the manuscript. Finally, we acknowledge M. Hafner and A. Wagner for making their scripts for robustness analysis publicly available.

■ REFERENCES

(1) Mann, S. (2012) Systems of creation: The emergence of life from nonliving matter. *Acc. Chem. Res. 45*, 2131−2141.

(2) Rafelski, S. M., and Marshall, W. F. (2008) Building the cell: Design principles of cellular architecture. *Nat. Rev. Mol. Cell Biol. 9*, 593−602.

(3) Fritz, B. R., Timmerman, L. E., Daringer, N. M., Leonard, J. N., and Jewett, M. C. (2010) Biology by design: From top to bottom and back. *J. Biomed. Biotechnol. 2010*, 232016.

(4) Semenov, S. N., Markvoort, A. J., Gevers, W. B. L., Piruska, A., de Greef, T. F. A., and Huck, W. T. S. (2013) Ultrasensitivity by molecular titration in spatially propagating enzymatic reactions. *Biophys. J. 105*, 1057−1066.

(5) Semenov, S. N., Markvoort, A. J., de Greef, T. F. A., and Huck, W. T. S. (2014) Threshold sensing through a synthetic enzymatic reaction−diffusion network. *Angew. Chem., Int. Ed. 53*, 8066−8069.

(6) Behar, M., and Hoffmann, A. (2010) Understanding the temporal codes of intra-cellular signals. *Curr. Opin. Genet. Dev. 20*, 684−693.

(7) Elowitz, M. B., and Leibler, S. (2000) A synthetic oscillatory network of transcriptional regulators. *Nature 403*, 335−338.

(8) Gardner, T. S., Cantor, C. R., and Collins, J. J. (2000) Construction of a genetic toggle switch in *Escherichia coli*. *Nature 403*, 339−342.

(9) Tabor, J. J., Salis, H. M., Simpson, Z. B., Chevalier, A. A., Levskaya, A., Marcotte, E. M., Voigt, C. A., and Ellington, A. D. (2009) A synthetic genetic edge detection program. *Cell 137*, 1272−1281.

(10) Schwille, P., and Diez, S. (2009) Synthetic biology of minimal systems. *Crit. Rev. Biochem. Mol. 44*, 223−242.

(11) Luisi, P. L., and Stano, P. (2011) Synthetic biology: Minimal cell mimicry. *Nat. Chem. 3*, 755−756.

(12) Soloveichik, D., Seelig, G., and Winfree, E. (2010) DNA as a universal substrate for chemical kinetics. *Proc. Natl. Acad. Sci. U.S.A. 107*, 5393−5398.

(13) Chen, Y.-J., Dalchau, N., Srinivas, N., Phillips, A., Cardelli, L., Soloveichik, D., and Seelig, G. (2013) Programmable chemical controllers made from DNA. *Nat. Nanotechnol. 8*, 755−762.

(14) Forster, A. C., and Church, G. M. (2007) Synthetic biology projects *in vitro*. *Genome Res. 17*, 1−6.

(15) Hodgman, C. E., and Jewett, M. C. (2012) Cell-free synthetic biology: Thinking outside the cell. *Metab. Eng. 14*, 261−269.

(16) Noireaux, V., Maeda, Y. T., and Libchaber, A. (2011) Development of an artificial cell, from self-organization to computation and self-reproduction. *Proc. Natl. Acad. Sci. U.S.A. 108*, 3473−3480.

(17) Niederholtmeyer, H., Stepanova, V., and Maerkl, S. J. (2013) Implementation of cell-free biological networks at steady state. *Proc. Natl. Acad. Sci. U.S.A. 110*, 15985−15990.

(18) Siegal-Gaskins, D., Tuza, Z. A., Kim, J., Noireaux, V., and Murray, R. M. (2014) Gene circuit performance characterization and resource usage in a cell-free "breadboard". *ACS Synth. Biol. 3*, 416−425.

(19) Franco, E., Giordano, G., Forsberg, P.-O., and Murray, R. M. (2014) Negative autoregulation matches production and demand in synthetic transcriptional networks. *ACS Synth. Biol. 3*, 589−599.

(20) Padirac, A., Fujii, T., and Rondelez, Y. (2013) Nucleic acids for the rational design of reaction circuits. *Curr. Opin. Biotechnol. 24*, 575−580.

(21) Yordanov, B., Kim, J., Petersen, R. L., Shudy, A., Kulkarni, V. V., and Phillips, A. (2014) Computational design of nucleic acid feedback control circuits. *ACS Synth. Biol. 3*, 600−616.

(22) Kim, J., White, K. S., and Winfree, E. (2006) Construction of an *in vitro* bistable circuit from synthetic transcriptional switches. *Mol. Syst. Biol. 2*, 68.

(23) Subsoontorn, P., Kim, J., and Winfree, E. (2012) Ensemble Bayesian analysis of bistability in a synthetic transcriptional switch. *ACS Synth. Biol. 1*, 299−316.

(24) Kim, J., and Winfree, E. (2011) Synthetic *in vitro* transcriptional oscillators. *Mol. Syst. Biol. 7*, 465.

(25) Franco, E., Friedrichs, E., Kim, J., Jungmann, R., Murray, R., Winfree, E., and Simmel, F. C. (2011) Timing molecular motion and production with a synthetic transcriptional clock. *Proc. Natl. Acad. Sci. U.S.A. 108*, E784−E793.

(26) Kim, J., Khetarpal, I., Sen, S., and Murray, R. M. (2014) Synthetic circuit for exact adaptation and fold-change detection. *Nucleic Acids Res. 42*, 6078−6089.

(27) Szostak, J. W., Bartel, D. P., and Luisi, P. L. (2001) Synthesizing life. *Nature 409*, 387−390.

(28) Gardner, P. M., Winzer, K., and Davis, B. G. (2009) Sugar synthesis in a protocellular model leads to a cell signalling response in bacteria. *Nat. Chem. 1*, 377−383.

(29) Weitz, M., Kim, J., Kapsner, K., Winfree, E., Franco, E., and Simmel, F. C. (2014) Diversity in the dynamical behavior of a compartmentalized programmable biochemical oscillator. *Nat. Chem. 6*, 295−302.

(30) Montagne, K., Plasson, R., Sakai, Y., Fujii, T., and Rondelez, Y. (2011) Programming an *in vitro* DNA oscillator using a molecular networking strategy. *Mol. Syst. Biol. 7*, 466.

(31) Padirac, A., Fujii, T., and Rondelez, Y. (2012) Bottom-up construction of *in vitro* switchable memories. *Proc. Natl. Acad. Sci. U.S.A. 109*, E3212−E3220.

(32) Padirac, A., Fujii, T., Estévez-Torres, A., and Rondelez, Y. (2013) Spatial waves in synthetic biochemical networks. *J. Am. Chem. Soc. 135*, 14586−14592.

(33) Hasatani, K., Leocmach, M., Genot, A. J., Estévez-Torres, A., Fujii, T., and Rondelez, Y. (2013) High-throughput and long-term observation of compartmentalized biochemical oscillators. *Chem. Commun. 49*, 8090−8092.

(34) Fujii, T., and Rondelez, Y. (2013) Predator−prey molecular ecosystems. *ACS Nano 7*, 27−34.

(35) Aubert, N., Mosca, C., Fujii, T., Hagiya, M., and Rondelez, Y. (2014) Computer-assisted design for scaling up systems based on DNA reaction networks. *J. R. Soc. Interface 11*, 20131167.

(36) Baccouche, A., Montagne, K., Padirac, A., Fujii, T., Rondelez, Y. Dynamic DNA-toolbox reaction circuits: A walkthrough. *Methods 67*, 234−249.

(37) Barkai, N., and Leibler, S. (1997) Robustness in simple biochemical networks. *Nature 387*, 913−917.
(38) Artyukhin, A. B., Wu, L. F., and Altschuler, S. J. (2009) Only two ways to achieve perfection. *Cell 138*, 619−621.
(39) Muzzey, D., Gómez-Uribe, C. A., Mettetal, J. T., and van Oudenaarden, A. (2009) A systems-level analysis of perfect adaptation in yeast osmoregulation. *Cell 138*, 160−171.
(40) Ma, W., Trusina, A., El-Samad, H., Lim, W. A., and Tang, C. (2009) Defining network topologies that can achieve biochemical adaptation. *Cell 138*, 760−773.
(41) Alon, U. (2007) Network motifs: Theory and experimental approaches. *Nat. Rev. Genet. 8*, 450−461.
(42) Novák, B., and Tyson, J. J. (2008) Design principles of biochemical oscillators. *Nat. Rev. Mol. Cell Biol. 9*, 981−991.
(43) Zhang, D. Y., and Winfree, E. (2009) Control of DNA strand displacement kinetics using toehold exchange. *J. Am. Chem. Soc. 131*, 17303−17314.
(44) Van Ness, J., Van Ness, L. K., and Galas, D. J. (2003) Isothermal reactions for the amplification of oligonucleotides. *Proc. Natl. Acad. Sci. U.S.A. 100*, 4504−4509.
(45) Hafner, M., Koeppl, H., Hasler, M., and Wagner, A. (2009) Glocal robustness analysis and model discrimination for circadian oscillators. *PLoS Comput. Biol. 5*, e1000534.
(46) Zamora-Sillero, E., Hafner, M., Ibig, A., Stelling, J., and Wagner, A. (2011) Efficient characterization of high-dimensional parameter spaces for systems biology. *BMC Syst. Biol. 5*, 142.
(47) Cellière, G., Fengos, G., Hervé, M., and Iber, D. (2011) The plasticity of TGF-ß signaling. *BMC Syst. Biol. 5*, 184.
(48) Basu, S., Mehreja, R., Thiberge, S., Chen, M.-T., and Weiss, R. (2004) Spatiotemporal control of gene expression with pulse-generating networks. *Proc. Natl. Acad. Sci. U.S.A. 101*, 6355−6360.
(49) Rodrigo, G., Carrera, J., and Jaramillo, A. (2007) Genetdes: Automatic design of transcriptional networks. *Bioinformatics 23*, 1857−1858.
(50) Dirks, R. M., Bois, J. S., Schaeffer, J. M., Winfree, E., and Pierce, N. A. (2007) Thermodynamic analysis of interacting nucleic acid strands. *SIAM Rev. 49*, 65−88.
(51) Zadeh, J. N., Steenberg, C. D., Bois, J. S., Wolfe, B. R., Pierce, M. B., Khan, A. R., Dirks, R. M., and Pierce, N. A. (2011) NUPACK: Analysis and design of nucleic acid systems. *J. Comput. Chem. 32*, 170−173.
(52) Hafner, M., Petrov, T., Lu, J., and Koeppl, H. (2011) Rational design of robust biomolecular circuits: From specification to parameters. In *Design and Analysis of Biomolecular Circuits: Engineering Approaches to Systems and Synthetic Biology* (Koeppl, H., Densmore, D., Setti, G., and di Bernardo, M., Eds.), pp 253−280, Springer, New York.
(53) Kirkpatrick, S., Gelatt, C. D., and Vecchi, M. P. (1983) Optimization by simulated annealing. *Science 220*, 671−680.
(54) Seeman, N. C. (1982) Nucleic acid junctions and lattices. *J. Theor. Biol. 99*, 237−247.
(55) Wakamatsu, T., Kitamura, Y., Kotera, Y., Nakagawa, N., Kuramitsu, S., and Masui, R. (2010) Structure of RecJ exonuclease defines its specificity for single-stranded DNA. *J. Biol. Chem. 285*, 9762−9769.
(56) Buchler, N. E., and Cross, F. R. (2009) Protein sequestration generates a flexible ultrasensitive response in a genetic network. *Mol. Syst. Biol. 5*, 272.
(57) Chen, D., and Arkin, A. P. (2012) Sequestration-based bistability enables tuning of the switching boundaries and design of a latch. *Mol. Syst. Biol. 8*, 620.
(58) Venturelli, O. S., El-Samad, H., and Murray, R. M. (2012) Synergistic dual positive feedback loops established by molecular sequestration generate robust bimodal response. *Proc. Natl. Acad. Sci. U.S.A. 109*, E3324−E3333.
(59) Rust, M. J., Markson, J. S., Lane, W. S., Fisher, D. S., and O'Shea, E. K. (2007) Ordered phosphorylation governs oscillation of a three-protein circadian clock. *Science 318*, 809−812.
(60) Rondelez, Y. (2012) Competition for catalytic resources alters biological network dynamics. *Phys. Rev. Lett. 108*, 018102.
(61) Hatakeyama, T. S., and Kaneko, K. (2012) Generic temperature compensation of biological clocks by autonomous regulation of catalyst concentration. *Proc. Natl. Acad. Sci. U.S.A. 109*, 8109−8114.
(62) Prindle, A., Selimkhanov, J., Li, H., Razinkov, I., Tsimring, L. S., and Hasty, J. (2014) Rapid and tunable post-translational coupling of genetic circuits. *Nature 508*, 387−391.
(63) Tu, Y. (2013) Quantitative modeling of bacterial chemotaxis: Signal amplification and accurate adaptation. *Annu. Rev. Biophys. 42*, 337−359.
(64) Knox, B. E., Devreotes, P. N., Goldbeter, A., and Segel, L. A. (1986) A molecular mechanism for sensory adaptation based on ligand-induced receptor modification. *Proc. Natl. Acad. Sci. U.S.A. 83*, 2345−2349.
(65) Goldbeter, A., and Koshland, D. E., Jr. (1984) Ultrasensitivity in biochemical systems controlled by covalent modification. Interplay between zero-order and multistep effects. *J. Biol. Chem. 259*, 14441−14447.
(66) Bray, D., Levin, M. D., and Morton-Firth, C. J. (1998) Receptor clustering as a cellular mechanism to control sensitivity. *Nature 393*, 85−88.
(67) Del Vecchio, D., Ninfa, A. J., and Sontag, E. D. (2008) Modular cell biology: Retroactivity and insulation. *Mol. Syst. Biol. 4*, 161.
(68) Hindmarsh, A. C., Brown, P. N., Grant, K. E., Lee, S. L., Serban, R., Shumaker, D. E., and Woodward, C. S. (2005) SUNDIALS: Suite of nonlinear and differential/algebraic equation solvers. *ACM Trans. Math. Software 31*, 363−396.